

Thermal Stability of Athermal ω -Ti(Fe) Produced upon Quenching of β -Ti(Fe)

Mario J. Kriegel,* Askar Kilmametov, Volker Klemm, Christian Schimpf, Boris B. Straumal, Alena S. Gornakova, Yulia Ivanisenko, Olga Fabrichnaya, Horst Hahn, and David Rafaja

This work shows the formation of the athermal ω phase in alloy Ti–4 wt% Fe. The alloy under study, heat treated at 800 °C for 100 h and subsequently water quenched, is investigated using X-ray diffraction (XRD), scanning electron microscopy (SEM), and transmission electron microscopy (TEM). The thermal stability of ω -Ti(Fe) is investigated by differential scanning calorimetry (DSC). The DSC measurements show a cascade of several thermic events between 160 and 450 °C, and one strong and sharp exothermic DSC peak at \sim 480 °C. The phase transformations and other microstructural changes behind these events are explained by complementary use of XRD, electron backscatter diffraction (EBSD), and TEM analyses that are performed on samples heated stepwise in the DSC apparatus. These experiments indicate that the embryos of athermal ω -Ti(Fe) grow up to \sim 400 °C and start to decompose into an α -Ti(Fe) + β assemblage already at 450 °C. At \sim 480 °C, the decomposition of the athermal ω -Ti(Fe) phase is practically finished. Thermal stability of athermal ω -Ti(Fe) is compared with the thermal stability of ω -Ti(Fe) produced in a high-pressure torsion (HPT) process, indicating a higher thermal stability of ω -Ti(Fe) in the non-deformed alloys.

1. Introduction

Due to their high strength, low density, and excellent corrosion resistance, titanium alloys are attractive materials for a variety of applications like aircrafts, aero-engines, biomedical devices, or components in chemical processing equipment.^[1] The properties of titanium alloys are further improved by alloying, which helps to control their phase composition and microstructure, in particular the phase transitions and the distribution of phases in the material. Titanium and titanium alloys crystallize in three allotropic modifications, which are i) the hexagonal closed packed (hcp) low-temperature α -Ti phase with the space group (SG) $P6_3/mmc$, ii) the body centered cubic (bcc) high-temperature β phase (SG: $Im\bar{3}m$), and iii) the hexagonal high-pressure ω phase (SG: $P6/mmm$).^[2] In addition, several metastable phases were reported in literature for Ti being alloyed with transition metals (e.g., V, Nb, Mo, Ta, Fe) as a result of quenching from a bcc-type β solid solution.^[3,4] In the Ti–Fe

system, the hexagonal close packed α' martensite (SG: $P6_3/mmc$) can be obtained after quenching if the iron content is low (≤ 5 wt% Fe).^[5–8]

The formation of the metastable ω phase (SG: $P6/mmm$) has been classified into two groups: athermal and thermally activated (isothermal). The athermal ω phase forms typically in a limited compositional range via a diffusionless, displacive collapse of the $\{111\}_\beta$ parent lattice planes of β through a shuffling mechanism.^[9,10] In contrast, the isothermal ω phase precipitates during annealing experiments involving diffusion processes (as a consequence of the diffusion of alloying elements).^[4,11] For Ti–Fe alloys, the formation of the athermal ω phase was reported to occur between 3 and 5 wt% Fe.^[3,4,8,11–13] For Fe contents higher than 5 wt%, the β phase is retained in the quenched sample as a metastable phase.^[3,11]

Only very little is known about the high-temperature stability of metastable phases, which are produced by quenching of Ti–Fe alloys. The stability of these phases (after water quenching) was investigated for only two alloy compositions (1 and 10 wt% Fe) by means of the thermal analysis upon heating.^[14] The presence of exothermal events in the differential scanning calorimetry (DSC)

Dr. M. J. Kriegel, Dr. V. Klemm, Dr. C. Schimpf, Dr. O. Fabrichnaya, Prof. D. Rafaja
TU Bergakademie Freiberg
Institute of Materials Science
09599 Freiberg, Germany
E-mail: Mario.Kriegel@iww.tu-freiberg.de

Dr. A. Kilmametov, Prof. B. B. Straumal, Dr. Yu. Ivanisenko, Prof. H. Hahn
Karlsruhe Institute of Technology (KIT)
Institute of Nanotechnology
76344 Eggenstein-Leopoldshafen, Germany

Prof. B. B. Straumal, Dr. A. S. Gornakova
Institute of Solid State Physics
Russian Academy of Sciences
142432 Chernogolovka, Russia

Prof. B. B. Straumal
National University of Science and Technology «MISIS»
119049 Moscow, Russia

The ORCID identification number(s) for the author(s) of this article can be found under <https://doi.org/10.1002/adem.201800158>.

DOI: 10.1002/adem.201800158

curves indicated several phase transformations, but the correlation of the phase transformations with the microstructure changes was not described yet.

Metastable β alloys exhibit excellent mechanical properties and a good formability, and offer the greatest flexibility for designing various microstructures due to the growth and precipitation of the α and ω phases, which are connected with the absorption/release of heat.^[15] Therefore, the present work is focused on the explanation of the correlations between the thermal events arising upon heating, phase transitions and microstructure changes.

In the as-quenched state, the samples under study contained 4 wt% Fe and consisted mainly of athermal ω . In a first step, they were investigated by DSC in order to get an overview of the transformation temperatures. Subsequently, the samples were heated stepwise to the desired temperatures and investigated ex situ using X-ray diffraction (XRD), transmission electron microscopy (TEM/HRTEM) with energy dispersive X-ray spectroscopy (EDS) and selected area electron diffraction (SAED). In addition, the spatial distribution of the phases after the decomposition process (heated up to 550 °C) were obtained by electron back-scatter diffraction (EBSD) experiments.

2. Experimental Section

The titanium alloy containing 4 wt% Fe (denoted Ti-4Fe) was prepared by inductive melting of high purity materials (99.9% Ti and 99.97% Fe) in high vacuum. The melt was cast in vacuum into a water-cooled copper crucible having a diameter of 10 mm. The as-cast cylinders were cut into disks with a thickness of approx. 1 mm. These disks were polished, etched, placed in silica ampoules, which were evacuated to a residual pressure of 4×10^{-4} Pa, sealed, annealed at 800 °C for 100 h, and subsequently quenched in room-temperature water (denoted as initial state). The annealing temperature of 800 °C was chosen slightly

below the β -solvus line (Figure 1a) to generate an α -Ti + β two-phase microstructure with the β phase as a major constituent. After the heat-treatment procedure, the oxygen content was determined by carrier hot gas extraction method using the analyzer G8 GALILEO (Bruker AXS GmbH, Germany) in a graphite crucible using He as the carrier gas. The measurements reveal very low oxygen contents of approx. 0.01 wt% after the annealing procedure.

The microstructure of the annealed and subsequently quenched samples (including the phase composition and the spatial distribution of the present phases) was investigated by means of optical, scanning electron microscopy, and electron back-scatter diffraction (OM, SEM, and EBSD, respectively). For these investigations, the samples were electropolished using the polishing device LectroPol-5 and the commercial electrolyte A-3 (both from Struers, Denmark). The SEM micrographs were taken using back-scattered electrons (SEM/BSE) with a FEG-SEM LEO 1530 GEMINI (Zeiss, Germany) operating at 20 kV. For the EBSD measurements, the acceleration voltage of 20 kV and the step size of 60 nm were chosen. The HKL Channel5 software was utilized to acquire and to index the EBSD patterns. Structure parameters needed to identify the Kikuchi patterns, that is, the space group and the lattice parameters, were taken from the ICSD^[16] database and from the analysis of the XRD patterns, respectively.

The phases present in individual samples subjected to different annealing temperatures were identified using X-ray diffraction (XRD). The XRD experiments were carried out in conventional Bragg–Brentano geometry (D8 Advanced, Bruker AXS, Germany) using Co- $K\alpha_1$ radiation (wavelength: 0.178897 nm) where a Johansson-type monochromator in the primary beam was used to suppress the spectral line Co- $K\alpha_2$. The X-ray tube was operated at 40 kV and 35 mA and scattered photons were detected using a LynxEye 1D detector. The analysis of the XRD patterns using the TOPAS^[17] software allowed to extract the lattice parameters of individual phases. Local analysis

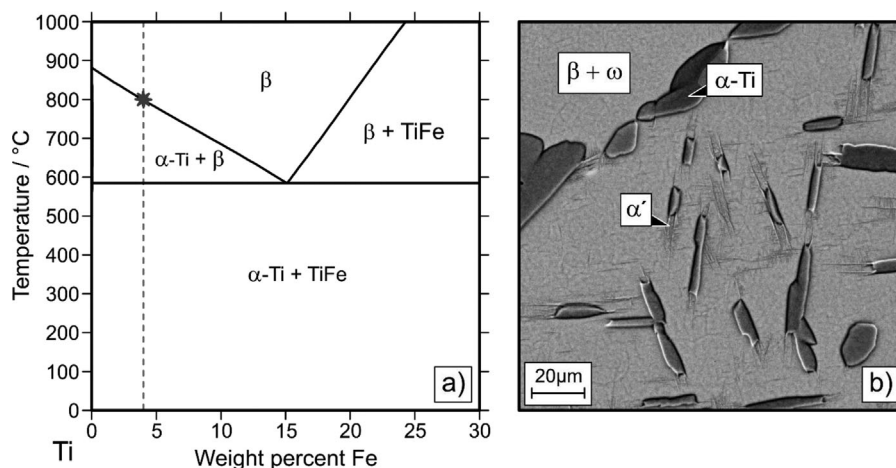


Figure 1. a) Ti-rich part of the binary Ti–Fe phase diagram calculated using the database recommended by SGTE.^[18] The position of the alloy Ti–4Fe at the annealing temperature of 800 °C is indicated by the asterisk symbol. b) A representative SEM/BSE micrograph of the water-quenched sample Ti–4Fe shows that the α -Ti and β phases are in equilibrium at the heat-treatment temperature of 800 °C. The α' -martensite plates and the athermal ω phase (not detectable by SEM/BSE) were formed upon quenching inside the β grains.

of the chemical compositions of the phases, the phase distribution and the analysis of the grain boundaries were done by transmission electron microscopy (TEM) using a JEM-2200FS microscope (JEOL, Japan), which was operated at 200 kV. The chemical compositions of each phase were analyzed using EDS in scanning TEM (STEM) mode, the phase identification was done using SAED and HRTEM. The TEM lamella was prepared by a lift-out technique using the focused ion beam (FIB) Helios NanoLab 600i (FEI, Netherland).

The thermal stability of athermal ω -Ti(Fe) was studied using a power-compensated differential scanning calorimeter DSC-8000 (PerkinElmer, United States). The DSC measurements revealed the temperatures of the phase transitions and the kind of heat events (endothermic/exothermic), which arise during heating the metastable states in the quenched samples. For the DSC measurements, the samples were placed in Pt crucibles with very thin Al_2O_3 inlets to avoid the direct contact between the metallic samples and the Pt crucible. Before each measurement, the system was flushed with high purity Ar (99.999% + Varian cleaning system) to remove remaining oxygen. The thermal analysis measurements were performed up to 250, 360, 450, 550, and 600 °C using heating/cooling rates of 10 K min⁻¹, respectively. The temperature calibration was executed using melting points of standard materials (indium and tin).

3. Results and Discussion

The annealing temperature (800 °C) was chosen according to the phase diagram of the binary Ti–Fe system to be located in the α -Ti + β two-phase region slightly below the β solvus line for 4 wt% Fe. The aim was to correlate compositional and structural differences of the metastable phases formed after quenching with the characteristics of the equilibrium phases. The phase diagram was calculated using a thermodynamic database recommended by the Scientific Group Thermodata Europe (SGTE).^[18] The Ti-rich part of the Ti–Fe phase diagram is shown in Figure 1a.

The SEM/BSE analyses of the quenched sample Ti-4Fe revealed that this sample possesses a two-phase α -Ti + β microstructure at the annealing temperature, where β is the major constituent. In addition, fine laths of α' precipitates were detected inside the β grains (Figure 1b). These α' precipitates form upon water quenching. The oxygen content of approx. 0.01 wt% was measured after the annealing procedure in the samples. As already shown by Y. Todaka et al.,^[19] a considerable oxygen content would impede the formation of ω -Ti(Fe).

The formation of ω -Ti(Fe) in the water-quenched sample was confirmed by SAED in the TEM. The intense spots in the SAED pattern (Figure 2a) can be indexed as reflections from β . The additional (not assigned) reflections, however, do not obey this metric, but they indicate a strong orientation relationship with β . The Fast Fourier Transformations (FFTs) of the local HRTEM micrographs (Figure 2c,d) revealed that the additional reflections stem from two variants of ω -Ti(Fe) with the orientation relationships i) $(1\bar{2}\bar{1})_\beta \parallel (03\bar{3}0)_\omega$ and $[101]_\beta \parallel [10\bar{1}0]_\omega$, and ii) $(1\bar{2}\bar{1})_\beta \parallel (011\bar{2})_\omega$ and $[101]_\beta \parallel [10\bar{1}0]_\omega$ to the parent β phase. The lattice parameters of ω -Ti(Fe) present in this sample are $a = (0.45960 \pm 0.00004)$ nm and $c = (0.28145 \pm 0.00004)$ nm as

determined using XRD (see below). The coincidence of crystal structures of ω and β is illustrated in Figure 2b. Obviously, these ω variants are twin related with the common twin plane $(10\bar{1})_\beta$ and $(011\bar{1})_\omega$ of the β and ω (Figure 2b, left variant) lattices, respectively. These orientation relationships are also consistent with the orientation relationship (OR) $(111)_\beta \parallel (0001)_\omega$ and $[\bar{1}\bar{1}0]_\beta \parallel [11\bar{2}0]_\omega$ reported in literature.^[3,4,11,20]

The analysis of the SAED patterns taken along the interface between $\beta + \omega/\alpha$ -Ti (Figure 3) showed that the reflections corresponding to ω are best developed in the interior of the former β grains, whereas they get diffuse toward the α -Ti grain boundary. The compositional analysis by EDS in STEM revealed that the concentration of iron in the $\beta + \omega$ region increases toward the $\beta + \omega/\alpha$ -Ti interface. While the Fe concentration in the interior of the former β grains was approx. 5 wt% Fe, it exceeded 10 wt% Fe at the interface between α -Ti and $\beta + \omega$. The comparison of the Fe concentration profile with the quality of ω diffraction spots confirms the former conclusions that the ω content increases as the Fe content approaches 4 wt%.^[21,22] In addition, this result is in accordance with conclusions from refs. ^[3,4,8,13] showing the formation of athermal ω in a limited compositional range between 3 and 5 wt% Fe. With increasing local Fe content, the crystal structure of ω becomes distorted, as it can be seen from the decreasing intensity and from the diffuse shape of the additional reflections belonging to ω -Ti(Fe). Consequently, the distorted ω phase resembles more and more β -Ti(Fe). Thus, the amount of the β phase apparently increases (Figure 3).

The main reason for the observed increase of the Fe concentration at the $\beta + \omega/\alpha$ -Ti interface is the formation of equilibrium α -Ti grains during the heat-treatment at 800 °C. As the solubility of Fe in α -Ti is almost zero (Figure 1a), the iron atoms are expelled from α -Ti into β . During the annealing, the iron atoms diffuse from the $\beta + \omega/\alpha$ -Ti interface toward the interior of the β grains. However, as the diffusion time is limited, the Fe concentration is not equalized. The orientation relationship between α -Ti and β at their interface, that is, $[101]_\beta \parallel [\bar{1}2\bar{1}\bar{1}]_\alpha$ and $(\bar{1}01)_\beta \parallel (10\bar{1}\bar{1})_\alpha$, that was concluded from the SAED patterns is shown in Figure 3c.

In the interior of the $\beta + \omega$ grains, the precipitation of fine laths of α' martensite was observed (Figure 3). The FFT of the HRTEM image (Figure 3d) shows that α' obeys the Burgers^[23] orientation relationship $[1\bar{1}\bar{1}]_\beta \parallel [11\bar{2}0]_{\alpha'}$ and $(110)_\beta \parallel (0001)_{\alpha'}$ as shown in ref. [24]. In addition, TEM/EDS measurements of the α' laths show decreased Fe solubility compared to the surrounding $\beta + \omega$ grain (not shown for sake of brevity).

The thermal stability of athermal ω -Ti(Fe) was investigated using DSC, which revealed a series of exothermal events (Figure 4). In order to be able to correlate these events with microstructure changes, another initial sample was successively heated in the DSC apparatus up to temperatures, which are slightly above the respective exothermic events (onset temperatures: 170, 230, 364, 484 °C), and investigated by means of post mortem X-ray diffraction. The heating and cooling DSC curves (heating/cooling rate of 10 K min⁻¹) are shown in Figure 4, the XRD patterns in Figure 5. The absence of the thermal events in the DSC cooling curves (inset in Figure 4) affirms the irreversible character of the reactions occurring upon heating. Thus, the XRD measurements after each DSC

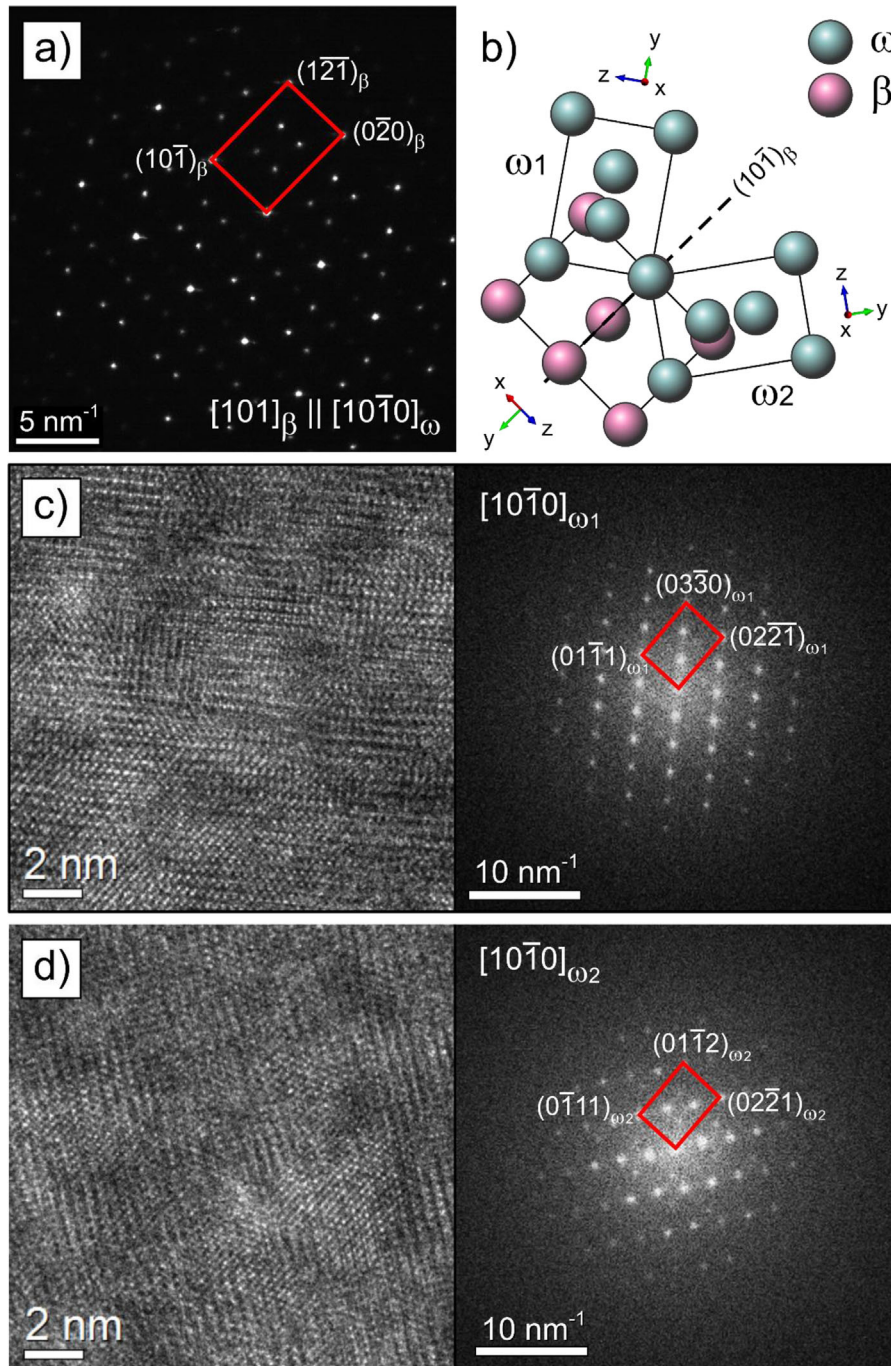


Figure 2. TEM investigations of Ti-4Fe (initial state). The TEM/SAED image a) shows the superposition of two ω variants together with β , whereas the red rectangle marks the diffraction spots corresponding to the reciprocal bcc cell. In b) the orientation relationship between β and the two ω variants is presented. The HRTEM images c) and d) with the corresponding FFTs show distinct areas where only one of these two ω variants is stable. The left and right ω variants in b) correspond to the FFTs of the HRTEM images c) and d), respectively.

scan can be directly correlated with the exothermic events upon heating in the DSC.

According to the XRD measurements (Figure 5a,b), the alloy Ti-4Fe contains a mixture of α -Ti and β in the as-quenched state. However, as only the diffraction line 110_{β} from the β phase was detected, it can be said that this phase is strongly disordered and

that a huge static Debye-Waller factor suppresses the subsequent diffraction lines. As the diffraction line 110_{β} from β coincides with the diffraction lines $10\bar{1}1_{\omega}$ and $11\bar{2}0_{\omega}$ from ω , it cannot be concluded, whether this diffraction line stems from β or from ω . The coincidence of the diffraction lines 110_{β} , $10\bar{1}1_{\omega}$, and $11\bar{2}0_{\omega}$ is perfect for $a_{\omega} = \sqrt{2}a_{\beta}$ and $c_{\omega} = (\sqrt{3}/2)a_{\beta}$.^[20,25,26]

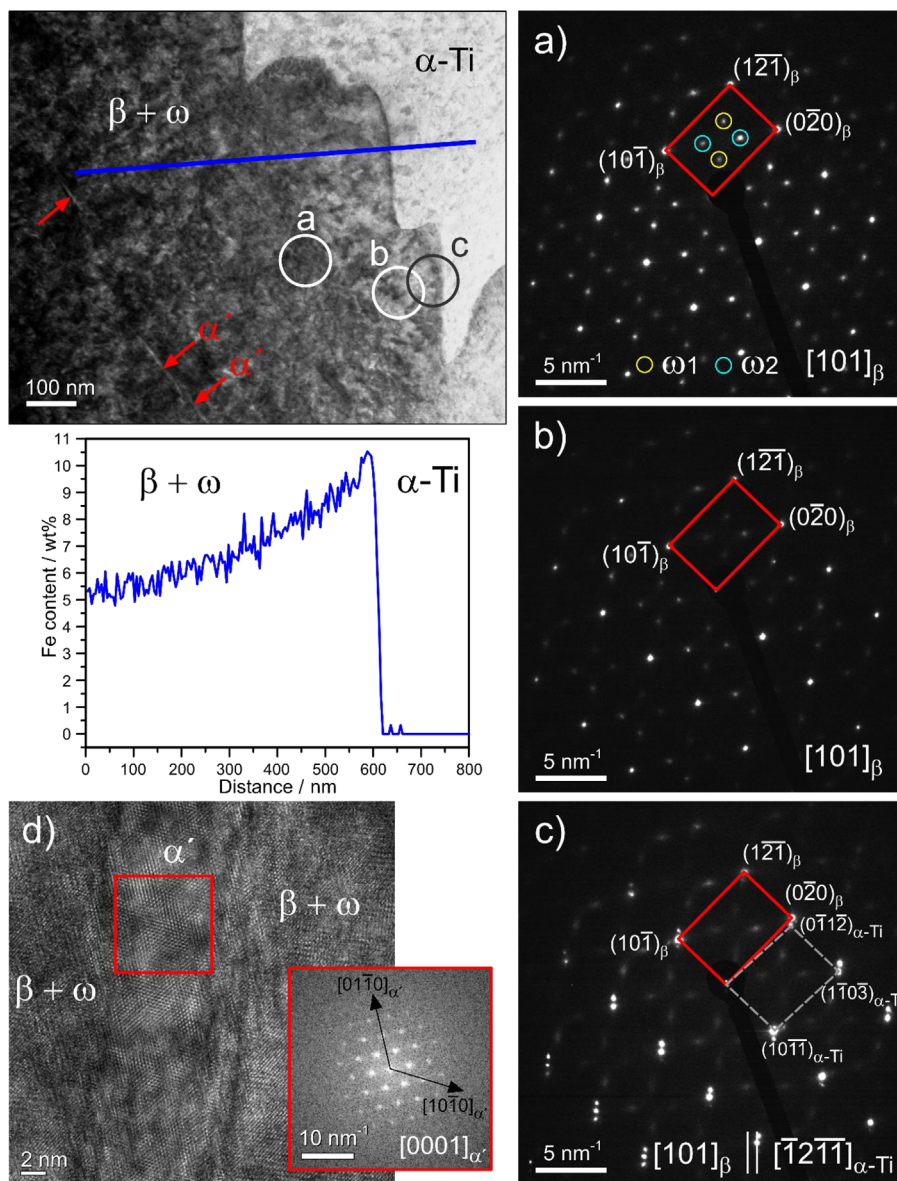


Figure 3. TEM investigations of Ti-4Fe (initial state) at the α -Ti + β grain boundary. The circles in the TEM/STEM image (top left) indicate the regions a), b), and c) of the respective SAED measurements shown on the right part of this figure, the blue line mark the EDS-line scan (shown below) and the arrows point at α' precipitates. In the TEM/SAED images the red rectangles and the dashed gray quadrangle indicate the reciprocal bcc and hcp sub-cells, respectively and the circles in a) mark the presence of two ω variants according to Figure 2. The TEM/HRTEM image d) with the corresponding FFT shows the formation of α' martensite inside former β grains (arrows in (a)).

The ω diffraction lines $11\bar{2}_\omega$ and $30\bar{3}1_\omega$, located at approx. $2\theta \approx 96^\circ$, which are not overlaid by any diffraction line of β , are not visible because of the structural disorder described above.

Upon heating the sample to 250 and 360 °C, the intensities of the $\beta + \omega$ peaks increased. The structural disorder was reduced, thus the peaks overlapping at approx. $2\theta \approx 96^\circ$, which are characteristic for ω , developed and its intensity increased continuously after sequential annealing up to 450 °C. This phenomena was usually associated with the formation of so-called isothermal ω .^[11,27,28]

The intense diffuse scattering visible on the left side of the $10\bar{1}1_\omega$ and $11\bar{2}_\omega$ peaks after annealing the sample at 450 °C

(Figure 5b) hints at the decomposition of ω and at the formation of β with a smaller lattice parameter and thus a higher Fe content as compared to the initial state. The change of the lattice parameter can be seen from the shift of the 110_β and 220_β peaks to higher diffraction angles after annealing the sample at 550 °C. After this annealing, no diffraction lines of ω were detected anymore.

Using published lattice parameters a_β of the solution phase β -Ti(Fe) from refs. [29–33] and a_{TiFe} of the intermetallic phase TiFe measured by Fischer et al.,^[34] the Fe content ($w(\text{Fe})$ in wt%) of β can be calculated by the application of Vegard's law^[35] using the linear lattice parameter dependence: $w(\text{Fe}) = -1688.4a_\beta[\text{nm}] + 553.6$ (Figure 6). The application of Vegard's law revealed the Fe

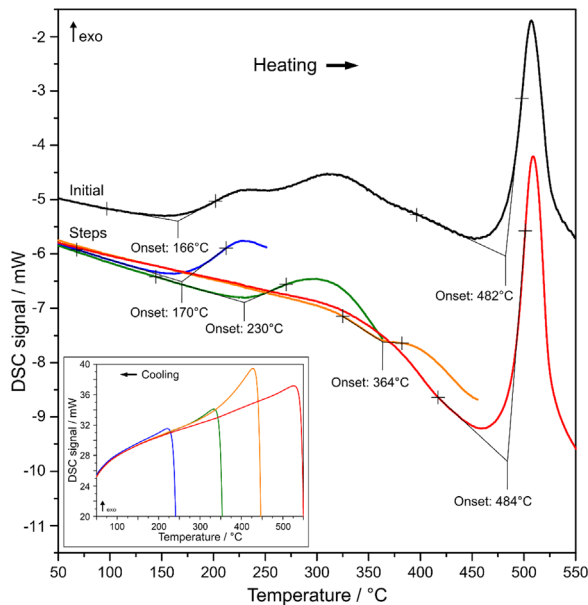


Figure 4. DSC measurements of Ti-4Fe using heating/cooling rates of 10 K min^{-1} showing i) a single heating run of the initial sample up to 600 °C and ii) stepwise measurements up to 250 , 360 , 450 , and 550 °C , respectively. The onset temperatures mark the transformation temperatures of the respective exothermic events upon heating. The inset in this figure show the cooling curves of the stepwise measurements.

content of approx. $10\text{--}14 \text{ wt\%}$ in the β phase after heating up to 550 °C ($a_{\beta} = 0.31962 \text{ nm}$). For the initial state, the Fe content in the β phase was estimated to be approx. $4\text{--}6 \text{ wt\%}$ ($a_{\beta} = 0.32498 \text{ nm}$), which is in agreement with the TEM/EDS observations (Figure 6).

Concurrently, the amount of α increased after the annealing up to 550 °C , as it can be seen on the splitting of the diffraction line 0002 from α . In accordance with the α' -martensitic phase, the diffraction lines of this newly formed $\alpha\text{-Ti(Fe)}$ phase are also shifted toward higher diffraction angles which indicates an increase in the Fe solubility compared to $\alpha\text{-Ti}$. This phase is denoted $\alpha\text{-Ti(Fe)}$ within the present work. In order to verify that variations of the chemical compositions are primary responsible for the shifts of the $\alpha\text{-Ti(Fe)}$ line positions, combined EBSD/EDS maps were recorded on Ti-4Fe after heating up to 550 °C as shown in Figure 6. The EBSD measurement was performed close to the $\alpha\text{-Ti}$ and β interface which were found to be in equilibrium at the heat-treatment temperature of 800 °C . After subsequent quenching and re-heating up to 550 °C former $\beta + \omega$ grains were found to be decomposed into a two-phase mixture containing $\alpha\text{-Ti(Fe)}$ and β . The EBSD/EDS measurement (Figure 7b) revealed that the newly formed $\alpha\text{-Ti(Fe)}$ phase is enriched by iron compared to the equilibrium $\alpha\text{-Ti}$ phase which can be seen in the XRD patterns as line shifts to higher diffraction angles. The decomposition of ω leads to the formation of $\alpha\text{-Ti(Fe)}$, which exhibits a smaller solubility of iron compared to ω . The β phase, which is already present in the initial state, accommodates the excess iron and is therefore stabilized below the eutectoid reaction temperature of 585 °C .^[18] Figure 7c shows the inverse pole figure map of $\alpha\text{-Ti}$ and $\alpha\text{-Ti(Fe)}$ revealing the

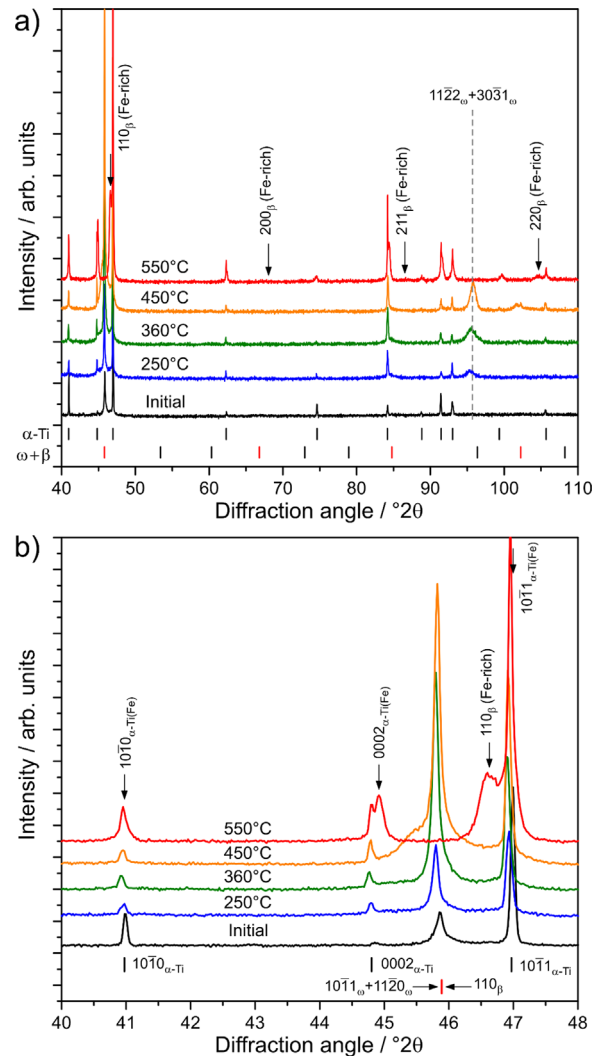


Figure 5. Comparison of the ex situ XRD measurements after stepwise heat-treatments of Ti-4Fe (initial state) up to 250 , 360 , 450 , and 550 °C . The diagram a) shows the whole measured diffraction patterns and b) enlarged parts between 40 and $48 \text{ 2}\theta$. The positions of the diffraction lines of $\alpha\text{-Ti}$, β (red markers) and ω (red and black markers) are indicated below the diffractograms. The formation of the Fe-rich β and $\alpha\text{-Ti(Fe)}$ phases after annealing up to 550 °C are indicated by the black arrows.

formation of several $\alpha\text{-Ti(Fe)}$ variants originating from one β grain which contains four ω variants. The nature of the decomposition mechanisms of ω to $\alpha\text{-Ti}$ was already discussed in literature.^[36–42]

- 1) The nucleation of α in the core of ω precipitates involves a displacive mechanisms^[40] or is developed directly from athermal ω with the help of vacancies,^[38] or
- 2) the ω to α phase transformation at β/ω interfaces is established by a coupled displacive-diffusional process,^[36,37,39] or
- 3) the α phase is formed due to a pseudo-spinodal decomposition process of β without any contribution of ω .^[41,42]

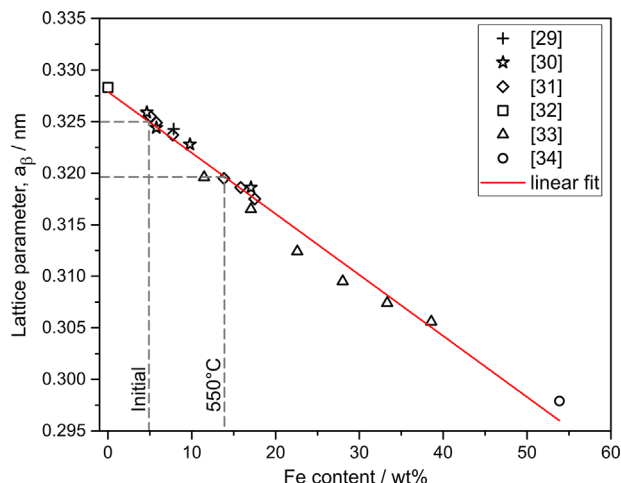


Figure 6. Variations of the lattice parameter a_{β} of β -Ti(Fe) with increasing iron solubility as shown by refs. [29–34]. The linear fit (red line) applied to the published data lead to the equation: $w(\text{Fe}) = -1688.4 a_{\beta} [\text{nm}] + 553.6$. The dashed gray lines indicate lattice parameters a_{β} measured for the initial state and after annealing up to 550°C .

Due to the lack of the lateral resolution of XRD in the direct space, it is difficult to conclude whether the phase transformation of α occurs at the β/ω interface or not. However, it was shown that the α phase transformation is directly related to the decomposition of ω (Figure 5) and that the diffusion process leads to the redistribution of iron and to the formation of α -Ti(Fe) and β -Ti(Fe) phases which contain more iron than equilibrium α -Ti and the metastable β -Ti phase after quenching.

Recently, several works investigated the phase transformations in the Ti–Fe system being induced by a high-pressure torsion process (HPT) and the thermal stability of the pressure

induced phases.^[14,21,22,43] The comparison of these findings with the results of the present work shows very interesting similarities in the transformation pathway upon heating, which will be discussed in the following.

In these works,^[14,21,22,43] it was shown that the transformation of α' and β to the high-pressure ω phase strongly depends on the iron composition. The smallest lattice mismatch between the β and ω lattices was found for an Fe content of approx. 4 wt%.^[21,22] Consequently, for this composition the transformation of $\beta \rightarrow \omega$ does not require mass transfer and thus just a small deformation (36° HPT rotation) is sufficient to transform β in this alloy almost completely to the ω phase. The studies of the thermal stability of HPT ω -Ti(Fe) revealed the transformation sequence $\omega \rightarrow \alpha$ -Ti(Fe) $\rightarrow \alpha$ -Ti + $\beta \rightarrow \beta$ upon heating.^[22] The DSC measurements performed in this work showed that the ω -Ti(Fe) phase transformation to an Fe-rich α -Ti(Fe) phase is an exothermic process occurring at approx. 380°C . With further temperature increase, above 650°C , this α -Ti(Fe) phase decomposes into the equilibrium phases α -Ti and β . This transformation was found to be endothermic and the transformation temperature decreases with increasing iron content in the sample. The observed heating curve of Ti–4Fe after annealing at 800°C and subsequent water quenching (initial state) also shows a cascade of exothermic events and one strong exothermic event at approx. 482°C (Figure 8). The comparison of the DSC measurements for the initial sample investigated in the present work and after deformation using HPT presented in ref.[22] reveal that the transformation temperatures upon heating are lowered by strong deformations and/or small grain sizes which are characteristic features of the microstructures after the HPT process. For the sample after HPT, the origin of the exothermic events with increasing temperature was correlated with defect annihilation and recrystallization processes, and the most dominant effect with the transformation of the metastable high-pressure ω phase to the supersaturated α -Ti(Fe) phase at

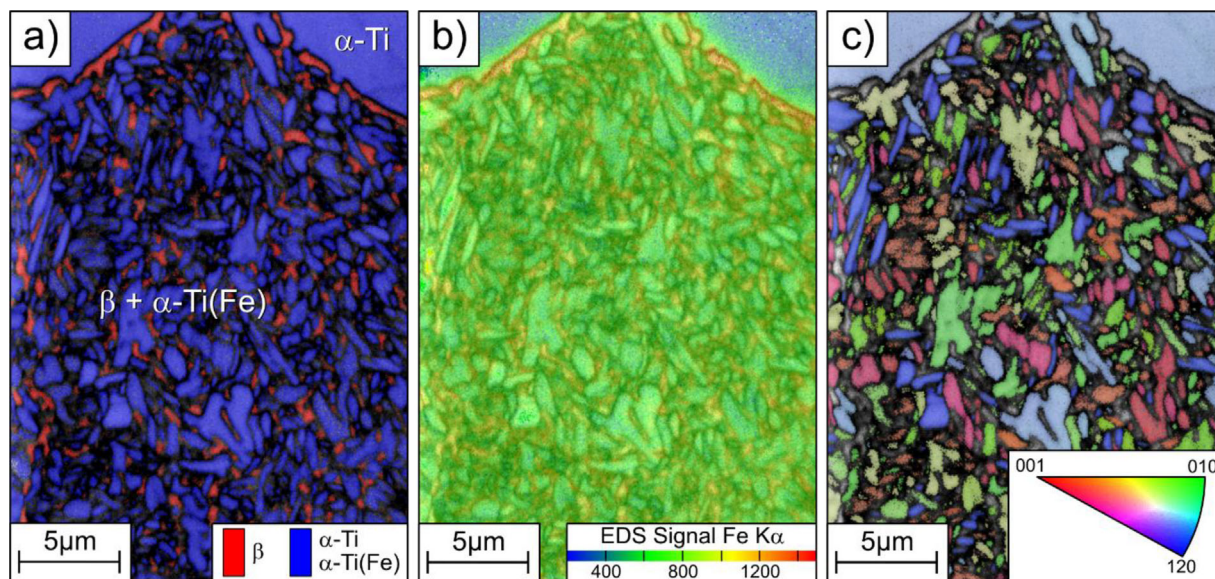


Figure 7. EBSD measurement at the α -Ti + β phase boundary after annealing of sample Ti–4Fe up to 550°C . In a) the EBSD phase map, in b) the EDS signal of Fe $K\alpha$, and in c) the inverse pole figure map of α -Ti and α -Ti(Fe), all superimposed on the band contrast image, are shown.

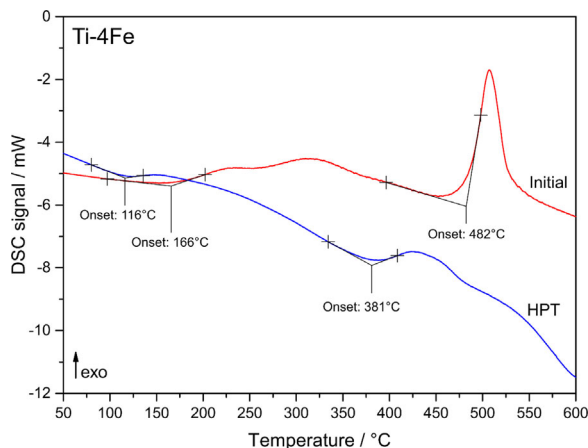


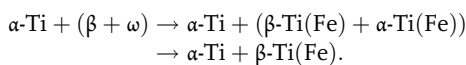
Figure 8. Comparison of DSC measurements of Ti–4Fe in the initial state and after deformation using HPT as published in ref. [22]. For the DSC measurements, heating rates of 10 K min^{−1} were applied.

approx. 381 °C.^[22] For the initial sample investigated in the present work, it can be concluded that the exothermic events (Figure 8) originate from the decomposition of the metastable phases such as athermal and/or isothermal ω inside the sample Ti–4Fe.

4. Conclusions

The initial microstructures of the titanium alloy containing 4 wt% Fe, which was annealed at 800 °C for 100 h and subsequently quenched in water, was investigated by means of X-ray diffraction, high-resolution TEM and selected area electron diffraction. The observations showed that the formation of athermal ω is favored inside metastable β grains with Fe contents of approx. 5 wt%. During heating in the DSC, the thermal stability of ω was investigated and correlated with ex situ XRD measurements. Up to 450 °C, the amount of ω increases with increasing temperature. At approx. 480 °C the decomposition of ω into an Fe-rich β and a supersaturated α -Ti(Fe) phase was observed to proceed as an exothermic event in the DSC.

In summary, the transformation path upon annealing of the quenched Ti–4Fe sample was found to be:



The comparison of the thermal stability of athermal ω -Ti(Fe) with the pressure induced ω -Ti(Fe) phase produced in a high-pressure torsion (HPT) process, indicates a higher thermal stability of ω -Ti(Fe) in the non-deformed alloys.

Acknowledgements

The authors would like to thank Th. Kreschel from the Institute of Iron and Steel Technology (TU Bergakademie Freiberg) for determination of the oxygen content in the samples by means of carrier hot gas extraction method. The work was partially supported by German Research Foundation (grant numbers FA999/1, IV 98/5, HA 1344/32, RA 1050/20),

Russian Foundation for Basic Research (grant numbers 16-53-12007, 16-03-00285, 18-03-00067), Ministry of Education and Science of the Russian Federation in the framework of the Program to Increase the Competitiveness of NUST “MISIS” and Karlsruhe Nano Micro Facility.

Conflict of Interest

The authors declare no conflict of interest.

Keywords

athermal ω , thermal analysis, transformation pathway, thermal stability, Ti-Fe

Received: February 14, 2018

Revised: August 20, 2018

Published online:

- [1] G. Lütjering, J. C. Williams, *Titanium*, Springer Berlin Heidelberg, Berlin, Heidelberg **2007**.
- [2] D. Banerjee, J. C. Williams, *Acta Mater.* **2013**, *61*, 844.
- [3] S. Banerjee, P. Mukhopadhyay, *Phase Transformations*, Vol. 12, Elsevier Science, Oxford, UK **2007**.
- [4] S. K. Sikka, Y. K. Vohra, R. Chidambaram, *Progr. Mater. Sci.* **1982**, *27*, 245.
- [5] J. L. Murray, *Bull. Alloy Ph. Diagr.* **1981**, *2*, 320.
- [6] A. V. Dobromyslov, V. A. Elkin, *Scr. Mater.* **2001**, *44*, 905.
- [7] I. Levi, D. Shechtman, *Metall. Trans. A.* **1989**, *20*, 2841.
- [8] M. M. Stupel, M. Ron, B. Z. Weiss, *J. Appl. Phys.* **1976**, *47*, 6.
- [9] D. De Fontaine, N. E. Paton, J. C. Williams, *Acta Metall.* **1971**, *19*, 1153.
- [10] J. C. Williams, D. de Fontaine, N. E. Paton, *Metall. Trans.* **1973**, *4*, 2701.
- [11] B. S. Hickman, *J. Mater. Sci.* **1969**, *4*, 554.
- [12] V. N. Moiseev, *Metalloved. Term. Obrab. Met.* **1969**, *2*, 335.
- [13] G. I. Nosova, N. B. D'yakonova, I. V. Lyasotskii, *Met. Sci. Heat Treat.* **2006**, *48*, 427.
- [14] B. B. Straumal, A. R. Kilmametov, Y. Ivanisenko, A. S. Gornakova, A. A. Mazilkin, M. J. Kriegel, O. B. Fabrichnaya, B. Baretzky, H. Hahn, *Adv. Eng. Mater.* **2015**, *17*, 1835.
- [15] B. Appolaire, E. Aeby-Gautier, M. Dehmas, A. Settefrati, M. Cottura, A. Finel, Y. Le Bouar, in *Proc. 13th World Conf. Titanium*, John Wiley & Sons, Hoboken, NJ **2016**, 463.
- [16] Inorganic Crystal Structure Database (ICSD) in *Fachinformationszentrum Karlsruhe & National Institute of Standards and Technology*, Vol. Version 2012-1, 2012.
- [17] A. A. Coelho, (Ed: B. A. GmbH), Bruker AXS GmbH, Karlsruhe **2014**.
- [18] Scientific Group Thermodata Europe (SGTE), Thermodynamic Properties of Inorganic Materials, Landolt-Börnstein Group IV, Subvolume B: Binary Systems in *Binary Systems, Part 3: Binary Systems from Cs–K to Mg–Zr* Vol. 19, Springer Berlin/Heidelberg, Aachen 2005.
- [19] Y. Todaka, J. Sasaki, T. Moto, M. Umemoto, *Scr. Mater.* **2008**, *59*, 615.
- [20] A. Devaraj, S. Nag, R. Srinivasan, R. E. A. Williams, S. Banerjee, R. Banerjee, H. L. Fraser, *Acta Mater.* **2012**, *60*, 596.
- [21] A. R. Kilmametov, Y. Ivanisenko, A. A. Mazilkin, B. B. Straumal, A. S. Gornakova, O. B. Fabrichnaya, M. J. Kriegel, D. Rafaja, H. Hahn, *Acta Mater.* **2018**, *144*, 337.
- [22] M. J. Kriegel, A. Kilmametov, M. Rudolph, B. B. Straumal, A. S. Gornakova, H. Stöcker, Y. Ivanisenko, O. B. Fabrichnaya, H. Hahn, D. Rafaja, *Adv. Eng. Mater.* **2018**, *20*, 1700933.
- [23] W. G. Burgers, *Physica* **1934**, *1*, 561.

- [24] C. M. Wayman, H. K. D. H. Bhadeshia, in *Physical Metallurgy*, Fourth, Revised and Enhanced Edition, (Ed: P. Haasen†), North-Holland, Oxford **1996**, 1507.
- [25] D. Ping, *Acta Metall. Sinica* **2014**, 27, 1.
- [26] J. M. Silcock, *Acta Metall.* **1958**, 6, 481.
- [27] T. W. Duerig, G. T. Terlinde, J. C. Williams, *Metall. Trans. A* **1980**, 11, 1987.
- [28] J. C. Williams, D. de Fontaine, N. E. Paton, *Metall. Trans.* **1973**, 4, 2701.
- [29] S. G. Fedotov, N. F. Kvasova, M. I. Ermolova, "Decomposition of the Metastable Beta Solid Solution of Titanium with Iron," presented at *Akademiia Nauk SSSR, Doklady* **1974**.
- [30] L. N. Guseva, L. K. Dolinskaia, *Akademiia Nauk SSSR, Izvestiia, Metall* **1974**, 195.
- [31] B. W. Levinger, *Trans. Am. Inst. Min. Metall. Eng.* **1953**, 197, 195.
- [32] B. W. Levinger, *J. Metals* **1953**, 5, 195.
- [33] R. Ray, B. C. Giessen, N. J. Grant, *Metall. Trans.* **1972**, 3, 627.
- [34] R. Fischer, W. Haelg, L. Schlapbach, F. Stucki, A. F. Andresen, *Mater. Res. Bull.* **1978**, 13, 931.
- [35] L. Vegard, *Z. Phys.* **1921**, 5, 17.
- [36] D. Choudhuri, T. Alam, Y. Zheng, R. Shi, S. Srivilliputhur, H. L. Fraser, R. Banerjee, in *Proc. 13th World Conf. Titanium*, John Wiley & Sons, Hoboken, NJ **2016**, 535.
- [37] T. Li, D. Kent, G. Sha, L. T. Stephenson, A. V. Ceguerra, S. P. Ringer, M. S. Dargusch, J. M. Cairney, *Acta Mater.* **2016**, 106, 353.
- [38] C. Lin, G. Yin, A. Zhang, Y. Zhao, Q. Li, *Scr. Mater.* **2016**, 117, 28.
- [39] S. Nag, R. Banerjee, R. Srinivasan, J. Y. Hwang, M. Harper, H. L. Fraser, *Acta Mater.* **2009**, 57, 2136.
- [40] F. Prima, P. Vermaut, G. Texier, D. Ansel, T. Gloriant, *Scr. Mater.* **2006**, 54, 645.
- [41] Y. Zheng, J. M. Sosa, R. E. A. Williams, Y. Wang, R. Banerjee, H. L. Fraser, in *Proc. 13th World Conf. Titanium*, John Wiley & Sons, Hoboken, NJ **2016**, 523.
- [42] Y. Zheng, R. E. A. Williams, J. M. Sosa, Y. Wang, R. Banerjee, H. L. Fraser, *Scr. Mater.* **2016**, 111, 81.
- [43] A. Kilmametov, Y. Ivanisenko, B. Straumal, A. A. Mazilkin, A. S. Gornakova, M. J. Kriegel, O. B. Fabrichnaya, D. Rafaja, H. Hahn, *Scr. Mater.* **2017**, 136, 46.